Influenza Neuraminidase Inhibitors: Structure-Based Design of a Novel Inhibitor Series

Vincent Stoll,[‡,§] Kent D. Stewart,*[,‡,§] Clarence J. Maring,[∥] Steven Muchmore,[‡] Vincent Giranda,[‡] Yu-gui Y. Gu,[∥] Gary Wang,[‡] Yuanwei Chen,[‡] Minghua Sun,[∥] Chen Zhao,[∥] April L. Kennedy,[∥] Darold L. Madigan,[∥] Yibo Xu,[∥] Ayda Saldivar,[∥] Warren Kati,[∥] Graeme Laver,[⊥] Thomas Sowin,[‡] Hing L. Sham,[∥] Jonathan Greer,[‡] and Dale Kempf[∥]

Departments of Advanced Technology and Anti-Infective Research, Abbott Laboratories,
100 Abbott Park Road, Abbott Park, Illinois 60064, and John Curtin School of Medical Research,
The Australian National University, Canberra 260, Australia

Received August 20, 2002; Revised Manuscript Received October 28, 2002

ABSTRACT: Combinatorial and structure-based medicinal chemistry strategies were used together to advance a lead compound with an activity of $K_i = 58$ μM via a potency enhancement of >70 000-fold to an analogue with an activity of $K_i = 0.8$ nM against influenza neuraminidase (A/Tokyo/67). Lead optimization was initiated using molecular modeling and combinatorial chemistry. Protein crystal structures revealed that inconsistent structure–activity relationship (SAR) data resulted from different binding orientations of the inhibitor core five-membered rings from one series to another. Binding modes for a series of compounds showed up to a 180° variation in orientation of the five-membered ring within the active site. Potent analogues were only achieved with chemical series that were observed to bind in the same orientation and yielded consistent SAR. In one series, consistent binding was obtained by an unprecedented occupation of a negatively charged binding pocket by a neutral methyl ester unit. The structural rationale for this novel SAR variation, based on protein crystallographic data, is given.

Influenza neuraminidase is an antiviral target of high pharmaceutical interest because of its essential role in cleaving sialic acid residues from cell surface glycoproteins and facilitating release of virions from infected cells (*1*). The three-dimensional structure of this protein was determined in the early 1980s (*2*) and played an important role in the discovery of two six-membered ring inhibitors, GG167 (zanamavir) and GS4071 (as its ethyl ester pro-drug, oseltamivir), which were approved in 1999 for treatment of influenza in the United States (see Table 1 for chemical structures) (*3*, *4*). Recently, we have described a new class of five-membered ring neuraminidase inhibitors (*5–7*). We report here details of our structure-based drug design effort to produce potent neuraminidase inhibitors.

Directed screening of selected chemical libraries using a neuraminidase biochemical assay identified a variety of compounds with activities less than 100 μM (*6*). One of these was a five-membered ring pyrrolidine-based inhibitor, **1**, with a K_i of 58 μM. Guided in part by molecular modeling, a combinatorial chemistry strategy for optimization was established which led to a 50-fold improvement in the inhibitor

potency to yield **2** with a K_i of 1.1 μM (*5*). Additional potency gains were elusive because of inconsistent structure activity relationship (SAR) of the compounds. Furthermore, modeling of this series ceased to be predictive. However, the availability of neuraminidase crystals into which inhibitors could be soaked (*8*) allowed the initiation of an iterative structure-based drug design program which used protein X-ray crystallographic feedback to provide structural features of some of these compounds. During this work, approximately 3–10 high-resolution (1.9–2.8 Å) compound-enzyme crystal structures were determined per week, typically with 12–24 h turn-around time. Ultimately >120 individual crystal structures were obtained in our research program. This throughput allowed the experimental evaluation of a large variety of synthetic analogues from different chemical series on a timely basis. The resulting iterative design cycles had a profound impact that permitted the rapid discovery of potent subnanomolar compounds. The crystal structures reported here provided both a rationale for otherwise unexplainable observations (vide infra) and confirmatory support for correct design predictions.

The neuraminidase active site is highly polar, with ten Arg, Asp, and Glu residues and four hydrophobic residues. To facilitate the discussion of the inhibitor binding modes, the active site is divided into 5 regions, termed subsites S1–S5. These subsites are diagrammed in Figure 1 and numbered in counterclockwise fashion using the crystal structure of the substrate-based inhibitor DANA (dehydro-deoxy-*N*-acetylneuraminic acid, structure shown in Table 1) bound to the active site (*9*). Site 1, S1, is comprised of three residues, Arg 118, Arg 292, and Arg 371, and provides a

* Corresponding author. Address: Building AP10, Department 46Y, 100 Abbott Park Road, Abbott Laboratories, Abbott Park, IL 60064-6100. Phone: (847) 937-1205. FAX: (847) 937-2625. E-mail stewartk@abbott.com.
‡ Department of Advanced Technology, Abbott Laboratories.
§ These two authors contributed equally to this manuscript.
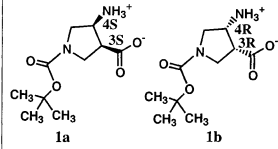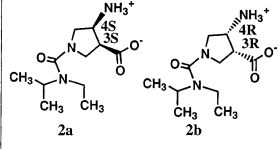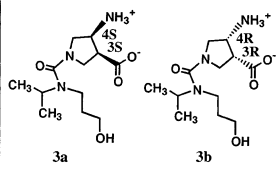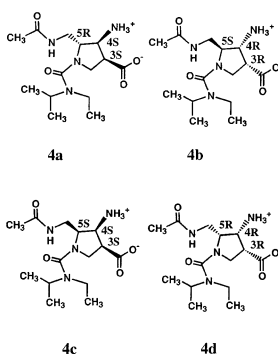∥ Department of Anti-Infective Research, Abbott Laboratories.
⊥ John Curtin School of Medical Research, The Australian National University.
[1] Abbreviations: N9, neuraminidase from A/tern/Australia/G70c/75 virus; N2, neuraminidase from A/Tokyo/67 virus; SAR, structure–activity relationship.
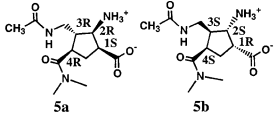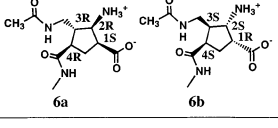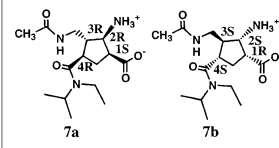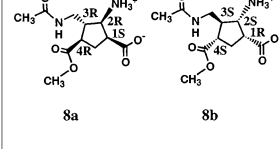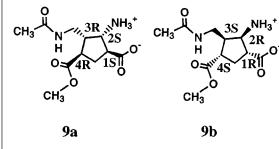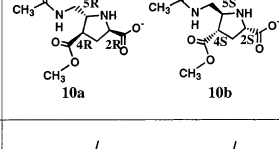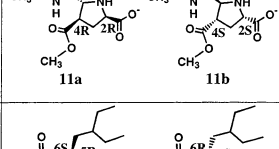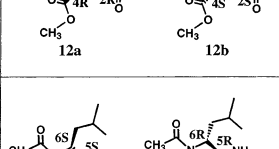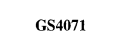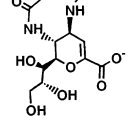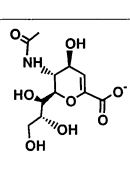
Table 1

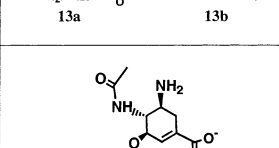| #	Compound Structure	Enzyme Assay Result		Crystallographic Result	
		Tested	Ki (μM)	Soaked	Observed
1	1a, 1b	Race-mate	58	Race-mate	1b
2	2a, 2b	Race-mate	1.1	not done	-
		Enan-tiomer 2a	57	not done	-
		Enan-tiomer 2b	0.5	Enan-tiomer 2b	Enan-tiomer 2b
3	3a, 3b	Race-mate	2.1	Race-mate	3b
4	4a, 4b, 4c, 4d	Dia-stereo-meric mixture of 4a-d in 3:3:1:1 ratio	6.3	Dia-stereo-meric mixture of 4a-d in 3:3:1:1 ratio	4a
		Race-mate 4a-b	4.4	not done	-
		Race-mate 4c-d	69	not done	-
5	5a, 5b	Race-mate	260	Race-mate	5a
6	6a, 6b	Race-mate	470	not done	-
7	7a, 7b	Race-mate	24	not done	-
8	8a, 8b	Race-mate	26	Race-mate	8a observed in two orientations
9	9a, 9b	Race-mate	0.7	Race-mate	9a
10	10a, 10b	Race-mate	0.9	Race-mate	10a
11	11a, 11b	Race-mate	0.037	Race-mate	11a
12	12a, 12b	Race-mate	0.0008	Race-mate	12a
13	13a, 13b	Race-mate	6.2	Race-mate	13a
	GS4071	Enan-tiomer	0.0002	Enan-tiomer	Result iden-tical to PDB entry 2QWK
	GG167	Enan-tiomer	0.0001	Enan-tiomer	Result iden-tical to PDB entry 1NNC
	DANA	Enan-tiomer	1.5	not done / PDB entry 1NNB was used	-

FIGURE 1: (A) Diagram of neuramindase active site with DANA inhibitor (from PDB entry 1NNB) showing the general location of sites S1—S5 and important nearby residues. (B) The corresponding protein picture showing the amino acid residues. Hydrogen bonds in S1, S2, and S5 are shown with dotted lines.

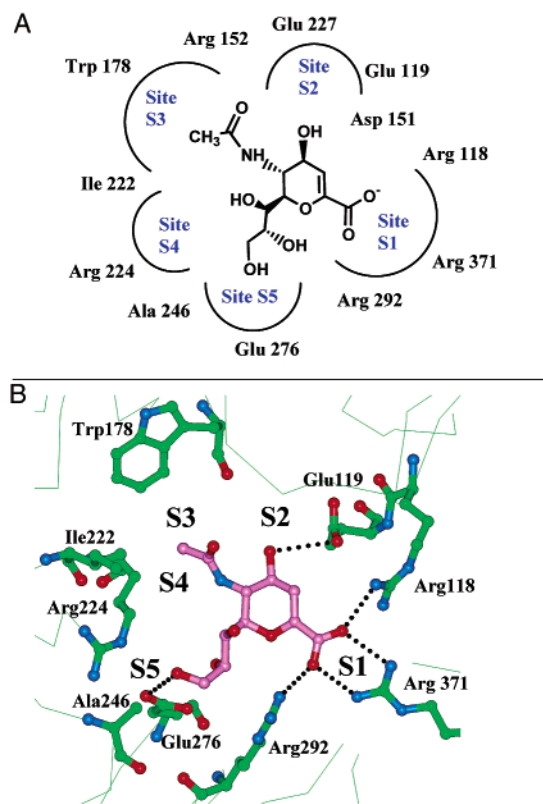positively charged electrostatic and hydrogen-bonding environment for anionic substituents from the inhibitor, such as carboxylate. Site 2, S2, is a negatively charged region of the active site and bounded by Glu 119 and Glu 227. Site 3, S3, contains a small hydrophobic region formed from the side chains of Trp 178 and Ile 222 adjacent to a polar region provided by the side chain of Arg 152 and a bound water molecule. Site 4, S4, is not occupied by any portion of the DANA inhibitor and is primarily a hydrophobic region derived from the side chains of Ile 222, Ala 246, and the hydrophobic face of Arg 224. Site 5, S5, is a region of mixed polarity and is comprised of the carboxylate of Glu 276 (trans conformation) and the methyl of Ala 246. As shown below and by others (*10*), Glu 276 can exist in an alternative gauche conformation with its carboxylate ion-paired with Arg 224. When Glu 276 is in this conformation, its methylenes join with Ala 246 to create a hydrophobic pocket within S5. An additional important active site residue is Asp151, and it is not formally part of the subsites as we have defined them. While the carboxylate of this residue does not make direct contact with DANA nor with the inhibitors of this report, Asp 151 is believed to play a critical role in catalysis by polarizing the scissile glycosidic linkage.

EXPERIMENTAL SECTION

Synthetic procedures for compounds **1**—**4** (*5*) and compounds **5**—**13** (*11*) have previously been described. Enzyme assays using A/Tokyo/67 neuraminidase were carried out at pH 6.5 according to literature protocol (*6*). All compounds were assayed as racemates unless otherwise indicated (see Table 1). Crystal structures of compounds **1**—**5** and **8**—**13** bound to neuraminidase were determined as described below, and coordinate files will be available from the Protein Data Bank upon publication. GG167 was generously provided by GlaxoSmithKline Co. GS4071 was synthesized according to literature procedure (*3*). The crystal structure of GS4071 bound to neuraminidase was identical to structure 2QWK independently determined (*12*) and deposited into the Protein Data Bank (*13*). DANA was purchased from Boehringer Mannheim GmbH.

Isolation, purification and crystallization of A/tern/Australia/G70c/75 neuraminidase was performed as reported (*8*). To prepare protein/ligand complexes, crystals were soaked in solutions of 0.93 M KH_2PO_4, 1.0 M K_2HPO_4, 3% dimethyl sulfoxide at pH 6.7 which contained millimolar concentrations (typically 30 mM) compound for 3—24 h. Crystals exposed to compound were then serially transferred into buffers containing 0%, 10%, 20%, and 27% glycerol for 1—2 min per step to prevent subsequent damage during the cryo-cooling process. Crystals were then frozen in a stream of 100 K nitrogen using an Oxford Cryo-stream cooling device. Diffraction data were recorded using either a RAXIS-IIc or MAR-130 image plate system on a Rigaku RU-2000 rotating anode X-ray generator operating at 100 mA and 50 kV. Diffraction data were reduced using DENZO (*14*), and the neuraminidase N9 model (accession number 1NNA) (*9*) from the Protein Data Bank (*13*) was used for initial phasing. Generation of initial electron density maps and structure refinement was achieved using the CNX program package (*15, 16*). Electron density maps were inspected on a Silicon Graphics Inc. workstation using the program QUANTA 97/2001 (Molecular Simulations Inc.), and the small molecule ligand structures fit to electron density. Structures were determined to a resolution of 1.95—2.5 Å and refined to R_{work} between 21% and 25% and R_{free} between 25 and 29%.

RESULTS

The pyrrolidine and cyclopentane-based compounds evaluated are listed in Table 1 along with their inhibitory potencies against type A neuraminidase. Since the stereochemical details of the compounds both as synthesized and as bound to the enzyme are particularly important, we have included separate columns within Table 1 that give the exact structure-(s) tested in the enzyme assay and the corresponding structure observed crystallographically to bind in the active site. The active site interactions of each inhibitor will be discussed below using the S1—S5 subsite nomenclature introduced above.

1. Evaluation of Screening Lead 1. Models of the two enantiomers of the screening lead **1** bound to the active site were prepared using the neuraminidase crystal structure (*2*) as template and manually docking an energy-minimized structure of **1** into a fixed (nonmobile) active site. Since the configuration of the active enantiomer was unknown at the time of modeling, both configurations were modeled, and the result for the *R,R* configuration **1b** is shown in Figure 2A. The *S,S* isomer **1a** binds similarly but with the orientation of the five-membered ring switched. The carboxylate was fit into S1, while the t-Bu group was oriented within the
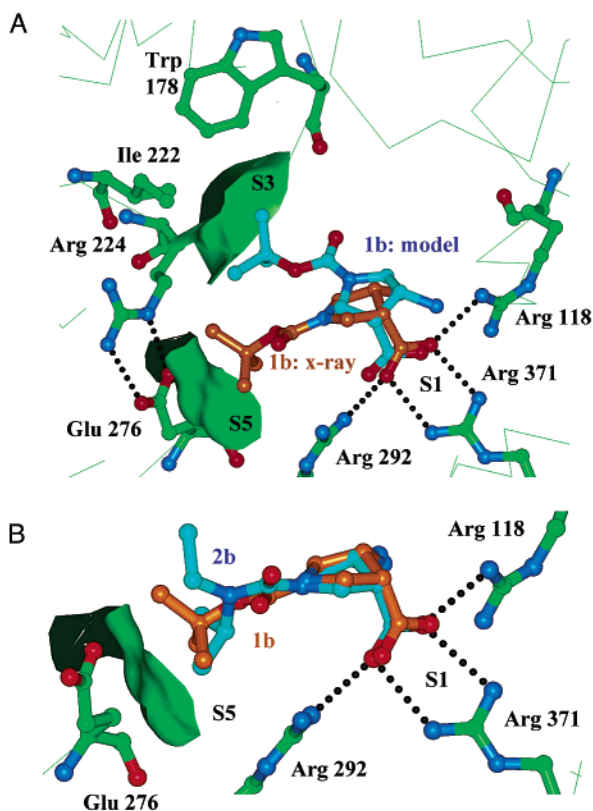
FIGURE 2: (A) Overlay of the model of **1b** (RR enantiomer, blue carbon atoms) and the X-ray crystal structure (orange) of **1b**. Hydrogen bonds in S1 are shown with dotted lines. The hydrophobic surfaces within S3 and S5 (Glu 276 in the bent conformation) are shown in green. (B) Close-up view of overlay of **1b** (orange carbon atoms) and **2b** (blue) crystal structures. The hydrophobic surface within S5 for Glu 276 in the bent conformation is shown in green.

hydrophobic portion of S3 so as to overlap with the hydrophobic region of the acetyl group of DANA. There were suboptimal contacts in the models of both enantiomers, and they were useful in the design of combinatorial libraries described below. The crystal structure of **1** (soaked as a racemate) determined subsequently showed that the *R,R* enantiomer, **1b**, as the active component. While the carboxylate bound as anticipated, the t-Bu group did not bind within S3 as modeled above, but instead bound within S5 making a hydrophobic interaction with the side chain methylenes of Glu 276 with its side chain bent in a gauche conformation. The overlay of modeled and observed structure **1b** is shown in Figure 2A. Importantly, the computer docking experiment using a nonmobile active site could not have anticipated this binding mode because of the conformational change of Glu 276.

2. Combinatorial Library Compounds, 2 and 3: Potency Gain for Unanticipated Reasons. On the basis of initial modeling of the two configurations of **1**, the proposed t-Bu interaction within S3 was judged to be suboptimal, and a round of combinatorial library exploration of urea analogues was evaluated with alternative alkyl groups. This produced optimized N-Et, N-*i*Pr analogue **2** with 55-fold increased potency at $K_i = 1.1 \mu M$ (5). Our inability to further increase the potency of this series caused us to question the accuracy of the models and prompted our first crystallographic determination of a member of this inhibitor series. Racemic **2** was separated into its two enantiomers with the two isomers

giving K_i values of 57 and 0.5 μM, respectively. The more active enantiomer was crystallographically studied bound to neuraminidase and determined to be the R,R enantiomer (Figure 2B). In contrast to the modeling of **1**, the N-Et, N-*i*Pr substituent of **2** was found to bind in S5 and not S3 as anticipated. As stated above, these results with **2** prompted the subsequent determination of the crystal structure of **1**. The two crystal structures of **1** and **2** were in accord with one another with the *R,R* configuration observed and the alkyl group (tBu in **1** and N-Et,N-*i*Pr in **2**) bound in S5. In parallel with this study of a purified enantiomer of compound **2**, a racemic mixture of a related and nearly equipotent analogue, **3** was also evaluated crystallographically (not shown). In this second instance of soaking a racemic mixture of an inhibitor, the *R,R* configuration was determined to be the configuration of the bound enantiomer for **3** with the i-Pr group in S5 and hydroxypropyl group extending into S4. Within the series of compounds **1**-**3**, the carboxylate bound within S1, and the short alkyl groups bound within S5 and S4, with no occupation of S2 or S3. The main protein−inhibitor contacts were derived from ring substituents of the inhibitors with no specific protein contacts with the ring atoms of the inhibitors, other than general VdW contacts with residue Tyr 406.

3. Tetra-Substituted Pyrrolidine 4: Filling an Empty Subsite Accompanied by a Switch in Inhibitor Chirality Preference. In the crystal structures of **1**, **2**, and **3** reported above, it was observed that S3 was unoccupied in each complex. To potentially increase potency, a new series of tetrasubstituted pyrrolidines was designed (strategy shown in Figure 3) that would append the acetamide fragment of DANA found in S3 onto the chemical nucleus of **2**, resulting in the design of compound **4**. Unlike the six-membered ring inhibitors, an extra methylene is required to span the required distance between the acetamide group and the core five-membered ring. This compound was initially synthesized and tested as a mix of four isomers, structures **4a**−**4d**, with the stereochemistry of the appended acetamidomethylene added to the 5-position of the ring in a 3:1 cis:trans ratio relative to the cis 4-amino and 3-carboxyl groups of **2** (see numbering in Table 1). Crystallographic analysis of **4** indicated that a single isomer bound to the active site with the acetamidomethyl substituent projecting into S3 analogous to the acetamide group of DANA (see Figure 3) as designed. Interestingly, however, protein crystallographic analysis clearly identified the configuration of the bound component of **4a**−**d** to be 3*S*,4*S*,5*R*, (i.e., **4a**), and opposite to that of **2** at ring positions 3 and 4! Further purification of this isomeric mixture **4a**−**d** yielded a pure diastereomer, racemate **4a/b**, with a minor increase in activity as expected for enrichment from a 75% diastereomerically pure sample to a >99% diastereomerically pure sample. The net potency decrease in switching ring configuration from compound **2** to compound **4** could be rationalized by observing that the core pyrrolidine ring of **4a** was rotated 90° from that of **2b**. This deviation in core ring orientation results in a significant alteration in the placement of the amine within S2 and the N-Et, N-*i*Pr substituents within S4 and S5. Although the proper orientation of the *N*-acetyl group was achieved, the resulting binding affinity from that designed interaction was more than offset by the loss of interactions of the other substituents and/or ring atoms with the remainder of the
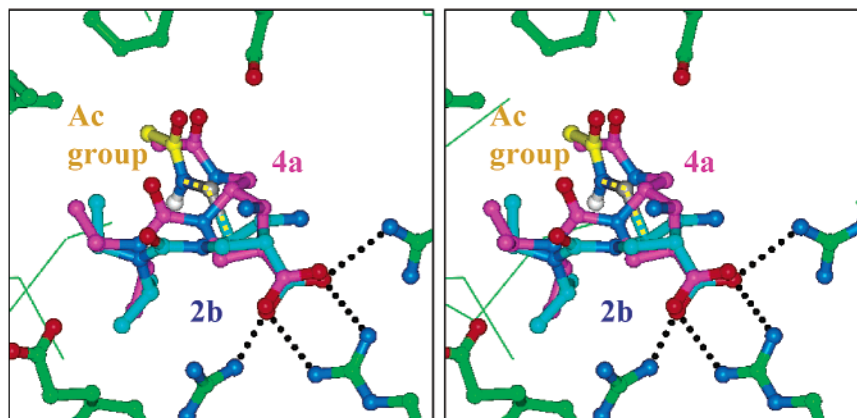
FIGURE 3: Stereoview of the design strategy leading to compound **4**. The crystal structure of **2b** (blue carbon atoms) and the acetamide fragment of DANA (Ac; yellow) are shown. The acetamide accepts an H-bond from Arg 152 and donates an H-bond to a water molecule (not shown). Hypothetical bonds linking the acetamide fragment with **2b** are shown with dashes via a methylene linker (grey atom). The crystal structure of compound **4a** (pink) is shown.

active site. It is unclear why the isomers of **4** that have 3*R*,4*R* ring configurations that correspond to compounds **1**−**3**, diastereomers **4b** or **4d**, do not bind, but a reevaluation of the initial model indicates that an unfavorable five-membered ring conformation may be required to permit simultaneous occupation of S1, S3, and S5.

4. The SAR of Cyclopentanes 5, 6, and 7 Parallels the Pyrrolidine Series. To further explore other core ring types that allowed projection of ring substituents into S4 and S5 by alternative vectors, cyclopentane analogues **5**−**7** were prepared. Compounds **5** and **6** have diminished hydrophobic interactions within S5 with their di- or monomethyl amide groups, respectively, and exhibit very weak activity with K_i = 470 and 260 μM, respectively. The crystal structure of **5** (not shown) indicated that its orientation within the active site was similar to that of **4** with one of the *N*-methyl groups making contact in S5 with the methylenes of Glu 276 in its bent side chain conformation. The direct cyclopentane analogue of pyrrolidine **4**, compound **7**, exhibits improved potency (K_i = 24 μM) relative to the methylated analogues **6** and **5** while slightly diminished relative to **4**. The trend in this series of amide analogues can readily be rationalized by the degree of hydrophobic interaction within S5, in analogy with that observed above for **1** and **3**.

5. Identification of a Novel Binding Mode: Compound 8. In striking contrast to the methyl amides above, methyl ester **8** with K_i = 26 μM was as potent as the most potent amide **7**. The unexpected potency of **8** was difficult to reconcile, given the small size and minimal hydrophobicity of the methyl ester within S5, and prompted the determination of its crystal structure of compound **8** bound to the enzyme (Figure 4A,B). While the observed electron density for the carboxylate, core ring and *N*-acetyl groups was clear, a single inhibitor orientation did not completely account for the observed density in S2 and S5. One orientation (A) put the methyl ester between S4 and S5 and the primary amine not reaching S2. This orientation did not provide a satisfactory fit to the observed electron density for the carboxylate in S1 and *N*-acetyl in S3. The second orientation (B) with the methyl ester in S2 and the amine projecting toward S5 gave a better fit to the observed electron density for the carboxylate in S1 and the *N*-acetyl in S3 but left the defuse density in S5 unoccupied. The second orientation (B) was initially
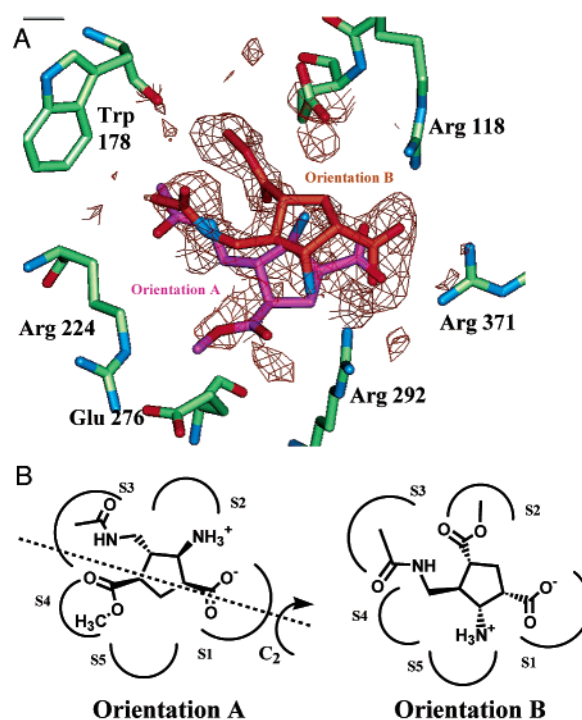
FIGURE 4: (A) Observed electron density for compound **8a** with orientation A (pink carbon atoms) and orientation B (orange) fit to the density (F_o−F_c map at 2.0 σ). (B) Diagram of binding orientations A and B for compound **8a.** The orientations are approximately related by a C_2 axis (shown in orientation A as a dashed line).

dismissed, however, because it placed a neutral methyl ester in the negatively charged S2−an interaction that was unprecedented and required a 180° rotation of the core ring orientation, relative to that observed for **4**. Orientation A was initially chosen for further design strategies because its binding orientation was closest to the orientation observed previously for **4** and **5**, and the poor fit of orientation A to the electron density was rationalized as disorder of a relatively weakly binding inhibitor. In orientation A, the amine is 2.7 Å from the corresponding primary amine of GS4071 in its bound structure and is clearly not making productive electrostatic interactions within S2.

FIGURE 5: (A) Crystal structure of **9a** showing occupancy of S1, S2, and S3 exclusively in orientation B. (B) Closeup of the methyl ester of **9a** binding in S2. The hydrophobic surfaces of Glu 119 and Glu 227 are shown in two shades of green.

FIGURE 6: Crystal structure of **10a** (orange carbon atoms) overlaid on the crystal structure of GS4071 (pink).

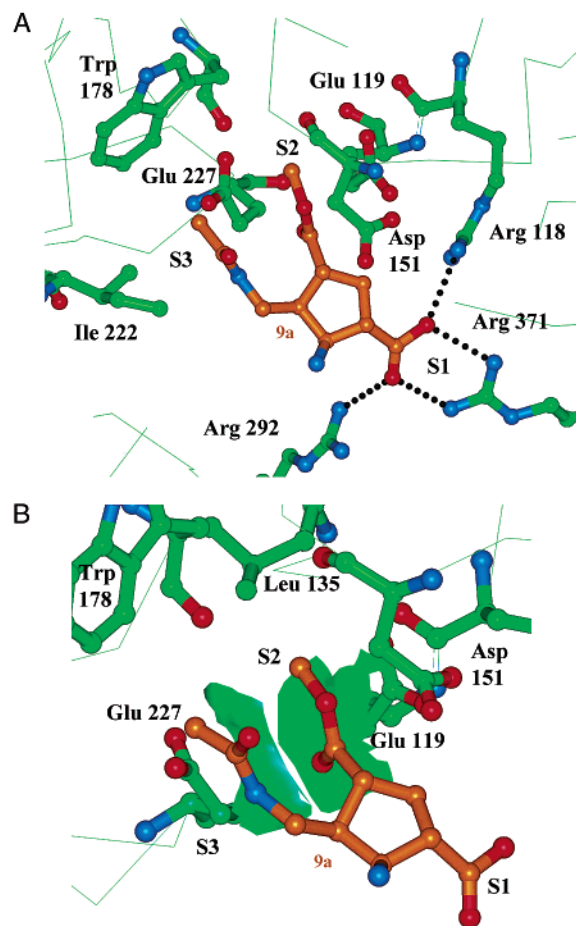*6. Confirming the Novel Ester Interaction in S2: Compound 9.* To better understand orientations A and B of **8** described above, diastereomeric analogue **9**, which had the primary amine epimeric in configuration was prepared. If this compound bound in orientation A, the amine was predicted to make improved electrostatic interactions with Glu119 in S2. If it bound in orientation B, the close VdW contact with Arg294 should be relieved. With a K_i of 0.7 μM, this compound exhibited a 30-fold gain in potency, relative to **8**, and was determined crystallographically to bind solely in orientation B with the methyl ester in S2, as shown in Figure 5A. A closeup of the methyl ester interaction with S2 is shown in Figure 5B. Importantly, compound **9** allowed our first unambiguous description of a methyl ester interaction within S2 with a potent compound that bound in a single orientation. As this nonpolar, non-positively charged interaction in S2 is unprecedented, the structural features are described in detail below (see Discussion section).

7. Optimizing Interactions within S5 Leads to Subnanomolar Analogue 12. The crystal structure of **9** and its initial SAR (CJM, unpublished results) suggested that the hydrophobic region of S4/S5 that is occupied by the 3-pentyl group of GS4071 was not easily accessible by appending groups to the primary amino function. Thus, in a parallel effort, we investigated an alternate series of pyrrolidine inhibitors typified by compound **10**. The potency of **10** was found to
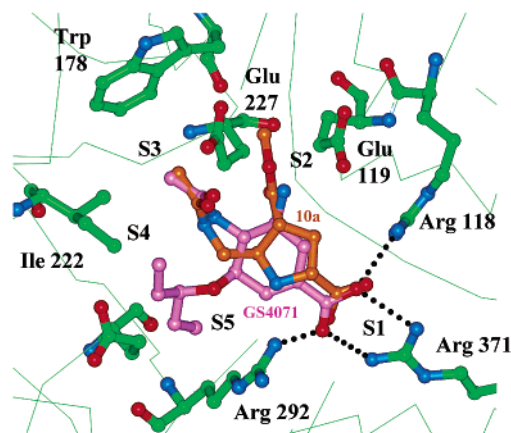
be equivalent to that of **9**, and its crystal structure, overlaid with GS4071, confirmed that alkyl substitution to project into S5 would be possible from the *N*-acetyl side chain (Figure 6). Pyrrolidine compounds **10**, **11**, and **12** show the potency improvement due to filling S5 with $-$H, $-$isobutyl, and 3-pentylmethylene with K_i values of 0.9, 0.037, and 0.0008 μM, respectively. Crystallographic analysis of **11** and **12** indicated that the compounds consistently bound in an orientation similar to that described above for **9** and **10** with their methyl esters bound within S2 (not shown). The isobutyl and 3-pentylmethylene units of **11** and **12**, respectively, occupy S4 and S5, as designed.

8. Direct Comparison of Amine vs Ester in S2 Shows True Potency Gain from Ester. To understand further the energetic value of positioning a methyl ester into S2, a site previously observed to bind cationic amine groups, the amine analogue of **11**, compound **13**, was prepared. Crystallographic analysis of **13** confirmed that the primary amine was oriented within S2. The SAR of the six-membered ring inhibitor series from which GG167 and GS4071 are derived indicates that placement of a cationic amine in S2 leads to a significant increase in inhibitory potency (4). The 170-fold potency loss for **13** in the five-membered ring pyrrolidine series, relative to the methyl ester **11**, indicates that there is significant binding contribution provided by the methyl ester unit and that the placement of the amine in **13** is not optimal. In accord with this dichotomy in SAR between the five-membered pyrrolidine series and the six-membered ring inhibitors, the amine of **13** differs in both position and orientation from the exo-cyclic amine of GS4071 being displaced by 1.0 Å and projected from the ring with the opposite stereochemistry (Figure 7).

DISCUSSION

This work describes the use of protein X-ray crystallographic information in the progression from a weak screening lead, **1** ($K_i = 58$ μM) to a potent subnanomolar inhibitor **12** ($K_i = 0.8$ nM). Crystal structures and knowledge of active site binding orientations of the bound inhibitors allowed an iterative feedback of structural information to complement the biological activity data and permitted efficient structure-based drug design. The lead compound, **1**, possessed a five-membered ring scaffold which was different from that of previously reported six-membered ring
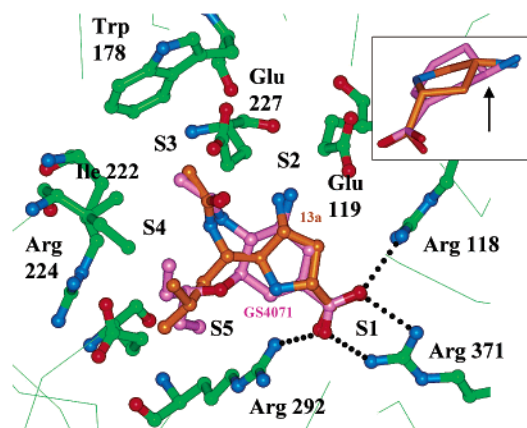
FIGURE 7: Crystal structure of compound **13a** (orange carbon atoms) overlaid with GS4071 (pink). Inset: View from right side of the two inhibitors (without the protein) showing the different projection vectors of the ring-amine bond. Only the ring subsubstituents in S1 (carboxylates) and S2 (amines) are shown.

inhibitors. While it is conceptually straightforward to imagine that a five-membered ring could mimic a six-membered ring compound, we found that the exact details of the substitution critically influenced the degree of potency and the binding mode of this series. Therefore, crystallographic evaluation of the binding mode(s) of the compounds proved invaluable for helping to guide the compound design. Recent work (*17, 18*) from other groups has also utilized a five-membered ring scaffold, but our work reported here represents independent observations and differs from the above in the observation of novel hydrophobic interactions in the S2 subsite—see below.

Our primary enzyme target was selected to be N2 neuraminidase because of the higher human infection rates from N2 viral serotypes. Our work on neuraminidases from viruses of other serotypes has been described previously (*5,7*). The ready availability, high stability, and facile soaking procedure of N9 neuraminidase crystals prompted us to use this alternate type A enzyme, N9. N2 and N9 are homologous enzymes, and bound inhibitor orientations have been shown to be similar (*9, 19*). Early studies of neuraminidase inhibitors had identified the unique and complimentary binding site for carboxylate-based inhibitors with the carboxylate positioned within S1, as shown in Figure 1B (*9*). From a subset of 300 organic carboxylates selected from our compound collection, compound **1** (structure shown in Table 1) was found to exhibit a K_i of 58 μM against N2 neuraminidase (*6*). The compound was a racemate of the cis-ring substituted isomer. In our initial work to exploit this lead compound, we had no information on the enantiomeric preference of binding, if any. Our early attempts to optimize this lead compound were based on molecular modeling studies of this lead compound (the crystal structure of **1** was determined at a subsequent time). The model of the t-Bu substituent bound in S3 indicated that t-Bu exceeded the available hydrophobic volume and that smaller alkyl groups such as Et or i-Pr might yield analogues of improved potency. This molecular modeling information was then used to design a combinatorial chemistry approach to optimizing the hydrophobic interaction of **1** with the protein. At the time of the modeling work, the only known hydrophobic region within the active site of neuraminidase was S3, and the t-Bu of **1** was assumed to bind within this region (Figure 2A). Optimization of the

hydrophobic interaction of **1** using parallel synthesis resulted in a compound with 55-fold improvement in potency (compound **2**); however, crystallographic analysis indicated this was due to interaction of the substituent within S5, rather than S3. An overlay of the modeled and experimental structures of **1** bound to neuraminidase is shown in Figure 2A. The observed orientation of the *tert*-butyl group near the hydrophobic methylenes of Glu 276 of S5 was unprecedented at that time and required a rotation of both χ_1 and χ_2 of the Glu 276 side chain by approximately 60°. Subsequently, other research groups have independently made similar observations regarding the two conformations of Glu 276 (*10*). From the crystal structure of **2** (Figure 2B), we concluded that within S5 it was possible to accommodate either polar units such as glycerol units of DANA that hydrogen bond to the "straight" conformation of Glu 276 or hydrophobic units such as the t-Bu of **1** that take advantage of hydrophobic interactions with the methylenes of "bent" Glu 276.

After establishing the correct binding mode for the close analogues **1**, **2**, and **3**, it was evident that none of these compounds occupied S2 and S3 of the active site, in contrast to six-membered ring inhibitors. Our strategy to improve potency of **2** was to append an acetamide substituent into S3. The designed compound, **4**, exhibited a 5-fold loss in potency relative to **2**, even though crystallographic analysis verified that S3 had been appropriately occupied (see Figure 3). Importantly, crystallographic analysis also indicated that the active component of **4** (compound **4a**) had the opposite enantiomeric configuration of the core ring compared to the active component of **2**. This unexpected switch in configuration produced a 90° change in the orientation of the core five-membered ring and significantly altered the vectors projecting from the ring into S2, S3, S4, and S5. Since these groups are no longer optimal in the new binding mode, the net potency gain for **4** over **2** was minimal despite the fact that the *N*-acetyl group bound in a similar orientation to the *N*-acetyl of DANA as designed. We speculate that a high-energy ring conformation prevented the binding of the isomer of **4** of ring configuration identical to **2**.

A third binding orientation for the five-membered ring inhibitor series was uncovered during the evaluation of compounds **8** and **9**. Figure 8 illustrates the 180° variation of central ring position for compounds of nearly equal, low-micromolar potency. It should be noted that the atoms of the core ring do not make any specific interaction with the protein; therefore, the orientations of the inhibitors are dictated primarily by the ring substituents that are present. The multiple binding modes made interpretation of SAR difficult and rational design strategies impossible to implement. For inhibitors that use specific hydrogen bonding interactions in only S1 and S3, there appeared to be an axis of rotation that could accommodate several core ring orientations, depending on the nature of the hydrophobic interaction in S5. This "axis" is diagrammed in Figure 4. While hydrophobic interactions in S4 and S5 are well-known to enhance potency, these sites were accessible via multiple vectors, and thus allowed various ring orientations. To "lock" into a single orientation, prevent oscillation and generate a consistent SAR, a specific interaction in an alternative off-axis location would be required. A three-site binding molecule could be obtained by adding interactions in any of
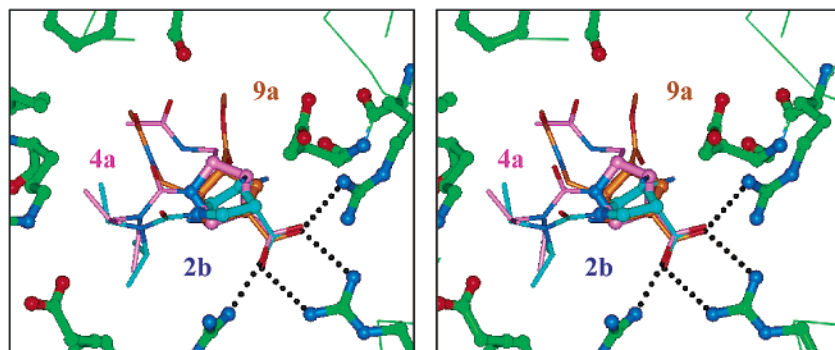
FIGURE 8: Stereoview of the overlay of crystal structures of compounds **2b** (blue carbon atoms), **4a** (pink), and **9a** (orange). The ring atoms are shown in thick ball-and-stick, and all ring substituents are shown in thin stick. These three inhibitors exhibit approximately equal enzyme inhibitory potency and have a 180° variation in orientation of their core five-membered rings due to multiple binding modes.

S2, S4, or S5 to compounds that already had optimized interactions within S1 and S3. S2 was selected for further design because of the excellent results reported previously for the six-membered ring compounds GS4071 and GG167. To achieve this, **8** (orientation A) was designed to project an amine toward S2, which preferentially binds a positively charged substituent in GG167 and GS4071.

Unexpectedly, the conserved binding orientation that we desired was achieved in compounds **8** and **9** by projecting the hydrophobic methyl ester into S2 instead of the amine. The interpretation of the electron density map of compound **8** bound to neuraminidase proved difficult. We initially attempted to fit the observed density to an orientation analogous to that of compound **4** (Figure 4, orientation A) with the carboxylate in S1, the acetyl in S3, and the methyl ester in S5. While this orientation fit some of the observed electron density, additional density remained in S2 near Glu 119 that was not readily explainable unless we invoked the unprecedented binding orientation B, which was contrary to established SAR precedent from the GG167 and GS4071 series of inhibitors. In orientation A, the exocyclic amine of **8** was positioned 2.7 Å distal from the corresponding amine position of GS4071 in S2 (presumed to be an optimal amine position). In an attempt to improve the amine position in S2, the epimer of **9** was designed and achieved a 30-fold potency gain, relative to **8**. Crystallographic analysis of **9** unambiguously indicated a single binding orientation with the methyl ester moiety bound in S2 (orientation B) and the core ring rotated from that of orientation A of **8**. This novel binding mode for **9** provided strong evidence that orientation B (Figure 4) was also the primary binding orientation for **8**. As will be shown below, methyl ester binding within S2 locked our core ring into a single orientation for ensuing analogues, compounds **10**-**13**, permitting significant advances in potency.

The observation of a methyl ester within S2 represents a novel finding and a significant paradigm shift in neuraminidase inhibitor design. Site S2 has traditionally been presented as a negatively charged pocket complementary to the binding of positively charged substituents. Close inspection of S2 reveals a remarkable balance of polar and charged residues via a hydrogen-bonding network. The results reported here indicate that S2 has more hydrophobic character than previously appreciated. Prior research had exploited the negative electrostatic character of S2 by design of comple-

mentary inhibitors containing a guanido, as in GG167, or amino, as in GS4071 (*3*, *4*). Buried salt interactions between the cationic group of the inhibitor and ionized carboxylates from Glu 119 and Glu 227 of the protein were invoked to rationalize the high potencies of these two inhibitors. A closer examination of this site reveals characteristics that allow for binding of hydrophobic substituents into this polar site (Figure 5B). The π-electron system of Glu 119 and Glu 227 carboxylates form part of the accessible surface area within this site. In addition, the CG of Glu 119, the CG of Glu 227, the CB of Asp 151, and CD1 of Leu 134 also contribute hydrophobic surface area to this region. Upon binding of the methyl ester of **9** within S2, the delocalized π-electron system of the $-COO-$ portion of the methyl ester stacks against the π-system of the carboxylate of Glu119, the ester methyl group contacts the CD1 of Leu 134, and the ester $-O-$ atom contact CB of Asp 151. In addition, two water molecules must be displaced from S2 upon binding of the methyl ester moiety. One water molecule is bound to Glu229, and the other is complexed between Glu227 and the backbone carbonyl of Trp178. Both of these water molecules are conserved in the bound structure of GS-4071. The displacement of these water molecules by the methyl ester of **9** presumably contributes to enhance potency via an entropic gain.

The novel binding of the methyl ester into S2 appeared to provide sufficient affinity to prohibit significant shifts in the binding of further analogues in this series. The bound orientations of the core five-membered rings of compounds **9**−**12** are nearly identical. This was one of our most critical achievements. As set out in our strategy outlined above, a consistent binding mode had been realized, leading to a potent inhibitor. In analogy with the published SAR of the GS4071 series (*3*), optimization of the S4/S5 interactions with the 3-pentyl analogue **12** produced subnanomolar enzyme inhibitor potency, $K_i = 0.8$ nM. While the potency of the racemate **12** approaches that of enantiomerically pure drugs GG167 and GS4071 (K_i values of 0.8, 0.1, and 0.2 nM, respectively), the methyl ester substituent within **12** is likely to be too labile for use of **12** as an orally bioavailable drug. Further investigation and exploitation of the novel hydrophobic character of S2 with inhibitors possessing methyl ester replacements which are stable in an in vivo environment has been described separately (*20*).

Finally, we sought to make a quantitative assessment of polar versus nonpolar interactions within the S2 in this series. Given the large (100−1000-fold) potency gains observed in six-membered ring inhibitors by changing a neutral hydroxy group to a cationic primary amine in GS4071 or to a cationic guanido group in GG167, it was necessary to establish what potency would be observed with a primary amine in the pyrrolidine series. As illustrated in Figure 7, compound **13** and GS4071 differ in both the position and projection vector of their primary amines in S2. The dramatic (170-fold) loss of potency observed with compound **13** relative to the neutral methyl ester analogue **11**, despite analogous binding modes, further illustrates the beneficial effect of the S2-methyl ester interaction for the five-membered ring series reported here.

CONCLUSIONS

We have described how the use of molecular modeling and protein X-ray crystallography combined with combinatorial and medicinal chemistry led from a 58 μM screening lead to a 0.8 nM inhibitor. This process has shown the critical impact that protein X-ray crystallography can have in accelerating the drug discovery process. This study also illustrates the strengths and limitations of molecular modeling in the absence of experimental structure determinations. Crystallographic feedback in a timely manner was critical for verifying our correct assumptions and understanding our unproductive design strategies. Multiple binding orientations of the core five-membered ring of the series made potency enhancement difficult and problematic; timely feedback with crystal structures (many in less than 24 h) allowed us to identify and adjust to these observations quickly. Unexpected binding modes identified in the crystal structures lead to major changes in the direction of the medicinal chemistry program. Compound mixtures, either racemates or diastereomeric mixtures, gave rise to confusing SAR because of the binding of opposite enantiomers in closely related analogues. Crystal structures enabled the identification of the active component from such mixtures (analogous to the procedure in CrystaLEAD) (*21*) avoiding time-consuming purifications or difficult enantiomeric syntheses/resolutions.

Accurate structural knowledge of the inhibitors bound to the active site made it clear that at least three regions of the active site of neuraminidase needed to be occupied to establish a consistent binding orientation, S1, S2, and S3, for our core five-membered ring. Establishing a consistent binding mode was critical to predictive structure-based drug design and discovering potent compounds in the nanomolar range that would potentially be useful for antiviral therapy. The observation of unexpected potency for **8** and the solution of its crystal structure allowed the discovery of a novel moiety bound into S2, which establishes a new paradigm for neuraminidase inhibitor design. The ability to determine large numbers of inhibitor/protein crystal structures in a timely manner allows for greater opportunities for understanding and identification of novelties that may be critical to the success of a drug discovery program. The research reported here was the structural basis for an extensive medicinal chemistry effort that has provided a clinical candidate compound (*7, 22, 23*).

REFERENCES

1. Air, G. M., Ghate, A. A., and Stray, S. J. (1999) *Adv. Virus Res. 54*, 375−402.
2. Varghese, J. N., Laver, W. G., and Colman, P. M. (1983) *Nature 303*, 35−40.
3. Kim, C. U., Lew, W., Williams, M. A., Liu, H., Zhang, L., Swaminathan, S., Bischofberger, N., Chen, M. S., Mendel, D. B., Tai, C. Y., Laver, W. G., and Stevens, R. C. (1997) *J. Am. Chem. Soc. 119*, 681−690.
4. von Itzstein, M., Wu, W.-Y., Kok, G. B., Pegg, M. S., Dyason, J. C., Jin, B., Phan, T. V., Smythe, M. L., White, H. F., Oliver, S. W., Colman, P. M., Varghese, J. N., Ryan, D. M., Woods, J. M., Bethell, R. C., Hotham, V. J., Cameron, J. M., and Penn, C. R. (1993) *Nature 363*, 418−423.
5. Wang, G., Chen, Y., Wang, S., Gentles, R., Sowin, T., Kati, W., Muchmore, S., Giranda, V., Stewart, K., Sham, H., Kempf, D., and Laver, W. G. (2001) *J. Med. Chem. 44*, 1192−1201
6. Kati W., Montgomery, D., Maring, C., Stoll, V. S., Giranda, V., Chen, X., Laver, W. G., Kohlbrenner, W., and Norbeck, D. W. (2001) *Antimicrob. Agents Chemother. 45*, 2563−2570
7. Kati W., Montgomery, D., Carrick, R., Gubareva, L., Maring, C., McDaniel, K., Steffy, K., Molla, A., Hayden, F., Kempf, D., and Kohlbrenner, W. (2002) *Antimicrob. Agents Chemother. 46*, 1014−1021
8. Laver, W. G., Coleman, P. M., Webster, R. G., Hinshaw, V. S., and Air, G. M. (1984) *Virology, 137*, 314−323.
9. Bossart-Whitaker, P., Carson, M., Babu, T. S., Smith, C. D., Laver, W. G., and Air, G. M. (1993) *J. Mol. Biol. 232*, 1069−1083.
10. Smith, P. W., Sollis, S. L., Howes, P. D., Cherry, P. C., Cobley, K. N., Taylor, H., Whittington, A. R., Scicinski, J., Bethell, R. C., Taylor, N., Skarzynski, T., Cleasby, A., Singh, O., Wonacott, A., Varghese, J., and Colman, P. (1996) *Bioorg. Med. Chem. Lett. 6*, 2931−2936.
11. Maring, C., Zhao, C., Stewart, K., Stoll, V.,Kati, W., Madigan, D., Sun, M., Xu, Y., Kennedy, A., Gu, Y., Krueger, A., Herrin, T., Laver, W. G., Saldivar, A., Montgomery, D., Muchmore, S., Kempf, D., and Kohlbrenner, W. (2000) New approaches for the inhibition of influenza neuraminidase, in *Proceedings of the Thirteenth International Conference on Antiviral Research*, Baltimore, MD.
12. Varghese, J. N., Smith, P. W., Sollis, S. L., Blick, T. J., Sahasrabudhe, A., McKimm-Breschkin, J. L., and Colman, P. M. (1998) *Structure 6*, 735−746
13. Berman, H. M., Westbrook, J., Feng, Z., Gilliland, G., Bhat, T. N., Weissig, H., Shindyalov, I. N., and Bourne, P. E. (2000) *Nucleic Acids Res. 28*, 235−242.
14. Otwinowski, Z., and Minor, W. (1997) *Methods Enzymol. 276*, 307−326
15. Brunger, A. T., Adams, P. D., Clore, G. M., DeLano, W. L., Gros, P., Grosse-Kunstleve, R. W., Ralf W., Jiang, J.-S., Kuszewski, J., Nilges, M., Pannu, N. S., Read, R. J., Rice, L. M., Simonson, T., and Warren, G. L. (1998) *Acta Crystallogr., Sect. D: Biol. Crystallogr. 54*, 905.
16. Badger, J., Berard, D., Kumar, R. A., Szalma, S., Yip, P., Griesinger, C., and Junker, J. (1999) *CNX Software Manual*, Molecular Simulations, Inc., San Diego, CA.
17. Babu, Y. S., Chand, P., Bantia, S., Kotian, P., Dehghani, A., El-Kattan, Y., Lin, T.-H., Hutchison, T. L., Elliott, A. J., Parker, C. D., Anath, S. L., Horn, L. L., Laver, G. W., and Montgomery, J. A. (2000) *J. Med. Chem. 43*, 3482−3486.
18. Chand, P., Kotian, P. L., Dehghani, A., El-Kattan, Y., Lin, T.-H., Hutchison, T. L., Babu, Y. S., Bantia, S., Elliott, A. J., and Montgomery, J. A. (2001) *J. Med. Chem. 44*, 4379−4392.
19. White, C. L., Janakiraman, M. N., Laver, W. G., Philippon, C., Vasella, A., Air, G. M., and Luo, M. (1995) *J. Mol. Biol. 245*, 623−634.
20. Maring, C., Krueger, A., Zhao, C., Sun, M., Madigan, D., Chen, H.-J., Yeung, M. C., Kati, W., Stewart, K., Stoll, V., Montgomery, D., Gu, Y., Kempf, D., Molla, A., Kohlbrenner, W., Kennedy, A., Herrin, T., Xu, Y., and Laver, W. G., (2000) Design, synthesis and activity of substituted pyrrolidine influenza neuraminidase

inhibitors, *Proceedings of the Thirteenth International Conference on Antiviral Research*, Baltimore, MD.

21. Nienaber, V., L., Richardson, P. L., Klinghofer, V., Bouska, J. J., Giranda, V. L., and Greer, J. (2000) *Nat. Biotechnol. 18*, 1105–1108.

22. Molla, A., Kati, W., Carrick, R., Steffy, K., Shi, Y., Montgomery, D., Gusick, N., Stoll, V. S., Stewart, K. S., Ng, T. I., Maring, C., Kempf, D. J., and Kohlbrenner, W. (2002) *J. Virology 76*, 5380–5386.

23. DeGoey, D. A., Chen, H.-J., Flosi, W. J., Grampovnik, D., Yeung, C. M., Klein, L. L., and Kempf, D. J. (2002) *J. Org. Chem., 16*, 5445–5453.

BI0205449